Preventing ASR-induced deteriorations with hydrophobic aggregates- a feasibility study

Isaac Offei [a], Aofei Guo [b,c,*], Zhihui Sun [a,*], Chengqing Qi [d], Noppadon Sathitsuksanoh [e]

[a] Civil and Environmental Engineering Department, University of Louisville, Louisville, KY 40292, USA
[b] School of Water Conservancy and Civil Engineering, Zhengzhou University, Zhengzhou 450001, Henan, China
[c] Yellow River Laboratory, Zhengzhou University, Zhengzhou 450001, Henan, China
[d] Ash Grove Cement Company, 11011 Cody Street, Suite 125, Overland Park, KS 66210, USA
[e] Chemical Engineering Department, University of Louisville, Louisville, KY 40292, USA

ABSTRACT

Concrete deterioration due to alkali-silica reaction (ASR) is one of the main durability concerns. This study explores the feasibility of minimizing ASR-induced deterioration by enhancing aggregates' hydrophobicity. Mortar samples with highly reactive aggregates were prepared. The aggregates were modified through coating with hexamethyldisilazane (HMDS) pretreated fumed silica for improved hydrophobicity. The ASR progression of the specimens prepared with nontreated (control-NHA), washed-coated (WHA), and non-washed coated aggregates (HA) was assessed using compressive strength, linear expansion, and dynamic modulus of elasticity tests. In addition, an ASR detection reagent was used to study the extent of deterioration of the mortar specimens. Furthermore, the microstructure and chemical compositions of the ASR-affected mortar were studied using scanning electron microscopy (SEM) and energy-dispersed X-ray analysis (EDX). The research found that although using hydrophobic aggregates may reduce the compressive strength, increasing the hydrophobicity of aggregates can significantly reduce ASR-induced expansion, minimize cracking, and prevent warping.

1. Introduction

Alkali-silica reaction (ASR) is a significant durability issue with concrete structures that receive practitioners' and researchers' attention. ASR is the reaction between alkaline pore solution in concrete and some phases of reactive silica in aggregates [1,2]. These reactive silica phases are usually chemically unstable. The reaction forms an alkali-silica gel, which distends by imbibing moisture to create internal pressure in concrete to induce expansion and cracks [3]. Consequently, it weakens the concrete, making it susceptible to other deterioration processes such as chloride penetration and steel corrosion [4,5]. Also, ASR can reduce concrete's mechanical properties (strength, Young's modulus, etc.) [6]. The severity of ASR on cementitious materials depends on the nature and amount of reactive silica present, with highly reactive phases capable of causing severe expansion [1]. The ASR-induced deteriorations typically take a long time to be visualized, usually after 5–15 years of construction, although the reaction may go on continuously or intermittently [7].

Research shows that the amount of moisture available, concrete constituents (reactive aggregates and cementitious materials), and alkalinity are the three critical factors affecting the nature and extent of ASR-induced deterioration [2,7]. Thus, the ASR prevention approaches that have been proposed have mainly targeted the elimination or reduction of these conditions. These ASR prevention approaches include using low alkali cement, non-reactive aggregates, supplementary cementitious materials (SCMs) such as slag and fly ash, and lithium-based admixtures [8–12]. Although promising results have been achieved with these strategies, there are some limitations to their full adoption. For instance, using non-reactive aggregates will help avert or prevent the occurrence of ASR in concrete; however, this is practically difficult since actual chemically inert aggregates are scarce in some regions [10,11]. Besides, some non-alkali reactive aggregates can still contribute to the alkalinity of concrete's pore solution [10]. SCMs such as fly ash have been harnessed to mitigate the effect of ASR in concrete [7]. However, availability issues hinder the usage of some of these SCMs in some regions due to restrictive environmental regulations [7,10,11]

* Corresponding authors at: School of Water Conservancy and Civil Engineering, Zhengzhou University, Zhengzhou 450001, Henan, China (A. Guo); Civil and Environmental Engineering Department, University of Louisville, Louisville, KY 40292, USA (Z. Sun).
E-mail addresses: a0guo003@zzu.edu.cn (A. Guo), z.sun@louisville.edu (Z. Sun).

or cost concerns. Moreover, some SCMs, particularly those with high calcium content, can release alkalis in the concrete pore solution, aggravating the alkali-silica reaction [10,11]. Thus, there is a need for alternative and sustainable materials and innovative approaches to ASR prevention.

While the mechanism of ASR formation is still poorly understood, researchers agree that moisture is one of the critical factors needed for deleterious ASR to occur [2,13–15]. Water enters the porous ASR gel, leading to swelling, expansion, and crack formation [10]. The moisture content of concrete necessary for ASR development is related to internal relative humidity (IRH), with the generally accepted critical IRH for deleterious ASR formation being over 80% [13,16]. Lindgård et al. [13] wrote that IRH might be influenced by the water-to-cement ratio (w/c) of concrete, porosity, and moisture state of the aggregates during mixing. Moisture's role in ASR is critical at the swelling and expansion stage and may transport different reactive species [4,13,17]. Since moisture is required for expansive ASR development, methods that seek to deprive concrete of water can mitigate the level of expansion [4,17]. Bérubé et al.[18] demonstrated this assertion by sealing concrete cylinders with silane, oligosiloxane, and polysiloxane and assessed their effectiveness against ASR-induced expansion and map cracking. At the end of their study, they reported that applying the sealants to the surface of the concrete cylinders reduced expansion and map cracking on their surfaces. The effectiveness of these sealants in reducing ASR expansion is attributed to the reduction of moisture uptake, which causes ASR gel expansion. Al-Rashed and Al-Jabari [19] also applied a dua-crystallization waterproofing penetrating material to the surface of freshly cast concrete and reported a promising reduction in ASR damages. However, a significant disadvantage of surface treatment is that they wear off over time [20], making moisture ingress possible for subsequent ASR expansion. In addition, if there is an internal source of moisture in the concrete, ASR can still fester even with the exterior surface treated [21].

Due to the possible loss of hydrophobicity for surface-treated concrete, other researchers have integrated hydrophobic materials such as silane emulsions, waterborne stearic acid emulsions, waste rubber powders, and dual-crystalline, as admixtures in bulk concrete mixtures [20,22–24]. Hydrophobic materials impede capillary suction and weaken the molecular attraction between the liquid and substrate by increasing the contact angle to over 90°[25]. When water-repellent lining forms on the pore walls, the high contact angle or hydrophobic-ity makes it difficult for moisture penetration [26]. The results from other studies have shown significant improvement in the transport properties of cement materials with the incorporation of hydrophobic admixtures. For instance, Qu et al. [24] recorded a substantial reduction of 57% and 65% in capillary water absorption and chloride penetration, respectively, when they incorporated hydrophobic materials into the mortar mixture. This result suggests that incorporating hydrophobic materials may be effective in ASR prevention.

Since ASR gel forms and expands on the surface or inside of aggregates, applying hydrophobic material directly to aggregate to inhibit moisture penetration can be more effective in ASR prevention. Hence, this study explores the feasibility of preventing the ASR of cement mortar by altering the moisture path on the surface of the aggregate with hydrophobic silica. First, a water absorption test was conducted to assess the effectiveness of the hydrophobic aggregates in reducing moisture uptake and changing the moisture paths within the mortar samples. Mortar prisms and cubes were also prepared to assess their performance under ASR conditions, using the accelerated mortar bar expansion, dynamic modulus of elasticity, and compressive strength tests. In addition, optical microscopy, scanning electron microscopy (SEM), and energy-dispersive X-ray spectroscopy (EDX) were also used to characterize the microstructure and elemental composition of the ASR products. The study found that the pretreated hydrophobic aggregates significantly reduced ASR-induced expansion and cracking.

Table 1
Chemical composition of Type I/II Portland cement.

Chemical Composition	Wt.%
SiO_2	19.7
Al_2O	4.84
Fe_2O	3.05
CaO	62.62
MgO	4.00
SO_3	3.23
Na_2O	0.15
K_2O	0.49
Loss of ignition	1.21

2. Materials and experiments

2.1. Raw materials

The Type I/II Portland cement with a medium grain size of 11.4 μm and Blaine's surface area of 400.8 m^2/kg was used. According to ASTM C150, a 0.47 percent equivalent sodium oxide was calculated (Na_2O + $0.658K_2O$) based on the chemical compositions listed in Table 1[27–29]. In addition, hexamethyldisilazane (HMDS) treated hydrophobic fumed silica (CAB-O-SIL® TS-530 by Cabot Corporation) with a medium size of 25 μm and specific gravity of 2.2–2.3 was used in this study to coat the aggregates. The fourier transform infrared spectroscopy (FTIR) spectrum with a 400–4000 cm^{-1} wavenumber range of the hydrophobic silica powder is shown in Fig. 1. The bands at about 800 and 1100 cm^{-1} are caused by the siloxane (Si-O-Si) symmetric and asymmetric stretching vibrations, respectively [30–32]. Also, the symmetric band that occurs at 1382 cm^{-1} indicates the presence of CH_3 [33]. The peak at 2972 cm^{-1} corresponds to the C-H bond's stretching vibration, representing the CH_2 and CH_3 groups [32–34]. These organic alkyl groups have a fatty character and can be found in silanes and siloxanes hydrophobic materials [25].

2.2. Aggregate coating

Highly reactive aggregates (sand) from a western state (Idaho Falls) with a fineness modulus of 2.60 were used in this study. This highly expansive fine aggregate source has an C1260 expansion of 0.94% at 16-day and 1.34% at 30-day. When preparing hydrophobic aggregates, two methods was used. One group of aggregates was coated directly with the hydrophobic silica (denoted as HA), while the other group was washed and dried before coating (denoted as WHA) to enhance the bonding of the hydrophobic fumed silica on the aggregate surfaces. Fig. 2 captures the flow chart for preparing hydrophobic aggregates. Firstly, hydrophobic silica was mixed with acetone at a mass ratio 3:97 and then sonicated in a Fisher Scientific ultrasonic bath for 15 min. The sonication ensured a uniform dispersion of the hydrophobic silica in the acetone to obtain a hydrophobic gel. Then, the prepared highly reactive aggregates (raw or washed) were gradually poured into the gel and stirred with a rod for the hydrophobic silica gel to cover the sand particles. The sonication bath was then covered and left for 24 h. Subsequently, the excess gel was poured out, and the aggregates were left to air-dry to obtain the hydrophobic aggregates. Fig. 3 displayed the different behavior of uncoated (control, denoted as NHA) in Fig. 3a and washed and coated aggregates (WHA) in water (Fig. 3b). It should be noted that the color and behavior of both HA and WHA in water are the same. Therefore, a figure of HA is not shown repeatedly herein. As a demonstration, the effect of coating on the hydrophobicity of the aggregate surface is also shown in Fig. 4, where water droplets portray different contact angles for coated and uncoated surfaces.

2.3. Mixture proportions

A constant water/cement (w/c) ratio of 0.5 was used for all the
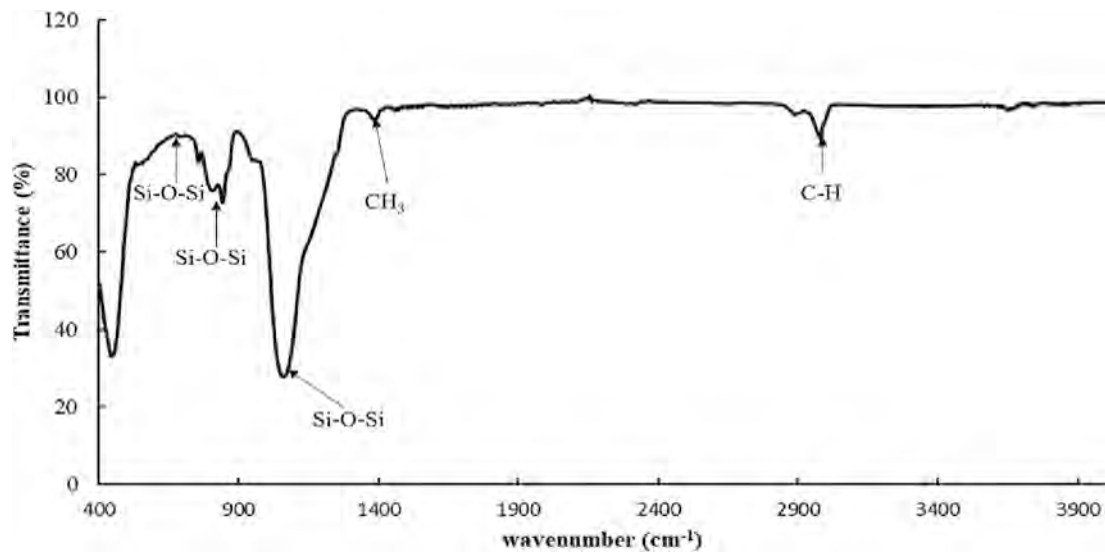
Fig. 1. FTIR spectrum for CAB-O-SIL® TS 530 hydrophobic silica.
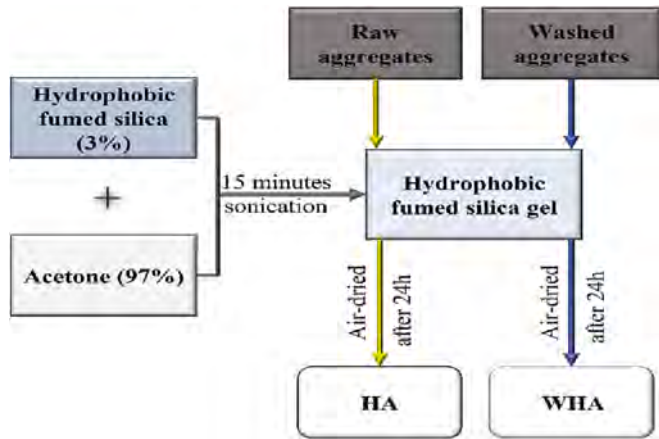
Fig. 2. Flow chart for preparing the hydrophobic aggregates.

samples. The mortar specimens were categorized into three groups, 0.5NHA, 0.5HA, and 0.5WHA, where 0.5NHA is the control mortar with raw aggregates (non-hydrophobic), 0.5HA is the mortar prepared with hydrophobic aggregates (direct coating, non– washed), and 0.5WHA is the mortar prepared with washed and coated hydrophobic aggregates. The mixture compositions and their respective proportions have been presented in Table 2.

2.4. Sample preparation

All the samples were prepared following the ASTM C 305 [35] using an ASTM-compliant Hobart laboratory mixer. Firstly, the cement and water were mixed for 1 min at a low speed. Afterward, all the measured amount of sand was added and mixed for an extra 1 min. Subsequently, the mixture was mixed for an extra 1 min at medium speed. Finally, the mixing machine was stopped for 1.5 min and then remixed for an additional 1 min to finish. The fresh mortar was then poured into steel molds of $50 \times 50 \times 50$ mm^3 cubes and $25 \times 25 \times 285$ mm^3 prisms for the compressive strength, expansion, and dynamic modulus of elasticity tests. All specimens were cured at 22 °C and relative humidity of 95% for 24 h before demolding for their assessments.
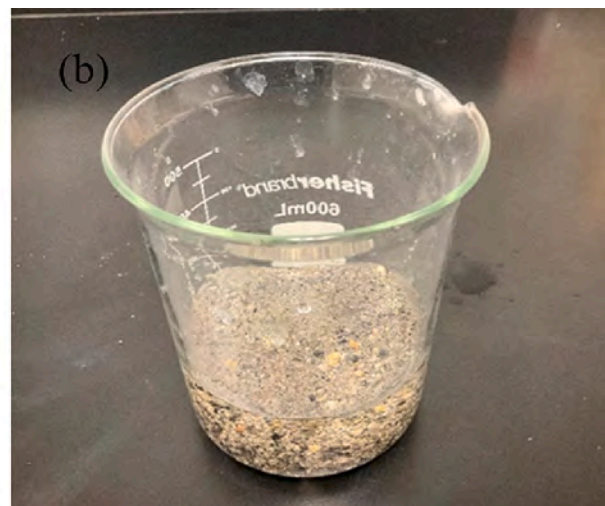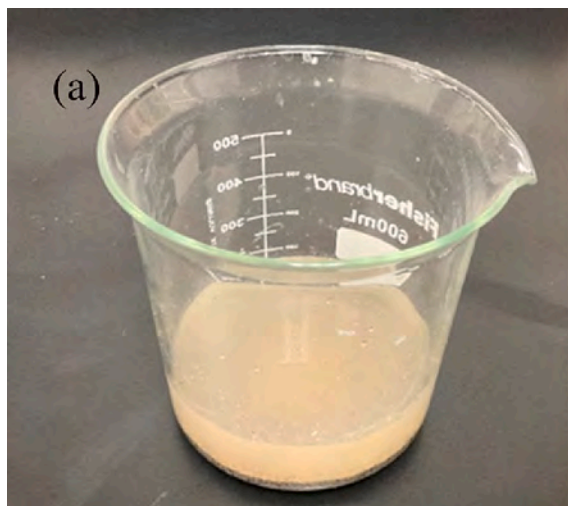
Fig. 3. Behavior of (a) NHA and (b) WHA underwater.
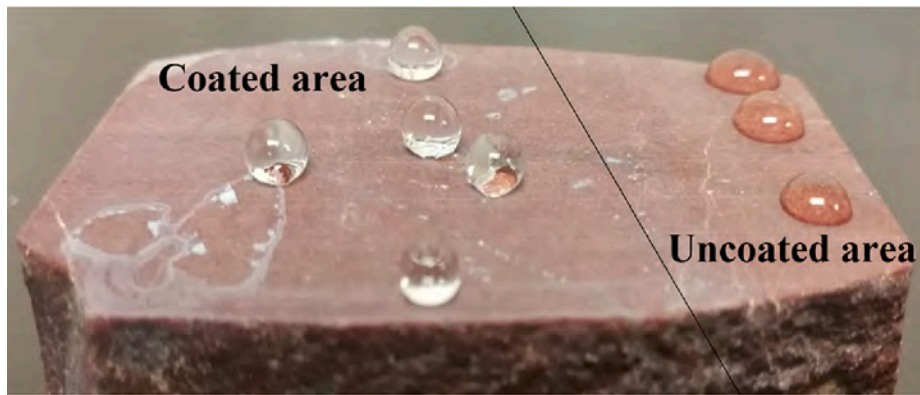
Fig. 4. Behavior of water droplets on coated and uncoated surfaces.

Table 2
Mixture proportions of mortars (by mass).

Mix composition	Water	Cement (g)	SAND (g)	Sand type
0.5NHA	0.50	1.00	2.25	NHA
0.5HA	0.50	1.00	2.25	HA
0.5WHA	0.50	1.00	2.25	WHA

2.5. Compressive strength test

The compressive strength test followed ASTM C109 [36] with a 267kN universal testing machine. For all the mortars listed in Table 2, the compressive strengths at 28 days cured under the mentioned conditions (22 °C and 95% relative humidity) were tested. Also, the compressive strength of the samples was tested on 3, 7, 14, and 28 exposure days of ASR-simulated conditions (80 °C, submerged under 1 N NaOH solution). Averages of 3 replicas at each test were recorded and denoted as the tested strength.

2.6. Dynamic modulus of elasticity test

The performance of the mortar prisms under the ASR-simulated conditions was also evaluated using the dynamic modulus of elasticity test, following the fundamental longitudinal frequency measurement approach using the resonant impact method outlined in ASTM C215 [37]. During the tests, the prisms of $25 \times 25 \times 285$ mm^3 ($1 \times 1 \times 11.25$ in^3.) were supported at their centers to allow free vibration in the longitudinal mode. One end of the specimens was attached with an accelerometer with a frequency range of 0.5–10 kHz was used for data acquisition. A rigid plastic stick was used to hit the other free end of the beams to generate vibrations (See Fig. 5). For every sample, the average of three fundamental longitudinal frequencies (n') corresponding to the maximum amplitude (peak) was used to calculate the dynamic modulus

of elasticity (E_d) (see Equation 1). Fig. 6 is a typical amplitude-frequency curve showing the peak amplitude and the corresponding fundamental frequency. Abnormally higher amplitude peaks usually occur at fundamental frequencies lower than 2000 Hz, which may be fraught with background noise. Thus, such amplitude peaks and their corresponding fundamental frequencies were ignored in calculating the E_d. The conditioning of specimens for the ASR test described by ASTM C1260 [38] was adopted for the dynamic modulus test. After demolding, the specimens were immersed in water at 80 °C (176°F) for 24 h before the zero reading. Subsequently, they were submerged in 1 N NaOH solution at 80 °C (176°F). The samples were taken out of the solution for daily measurement until 14 days under the solution.

$$E_d = DM(n')^2 \qquad (1)$$
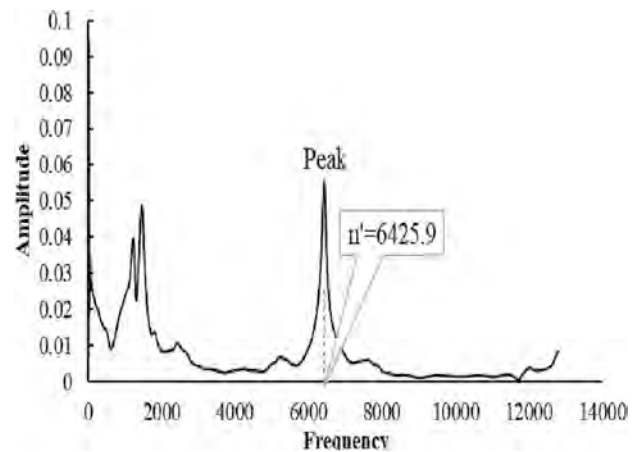
Fig. 6. Typical fundamental frequency vs. amplitude curve.
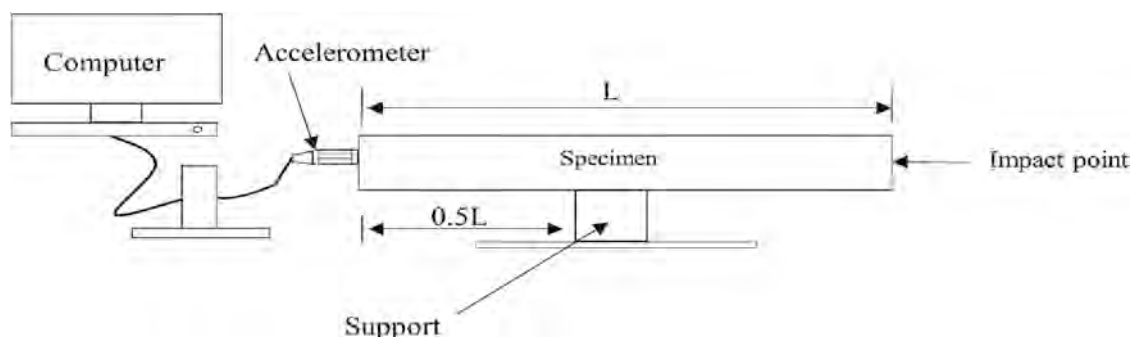
Fig. 5. Schematic diagram for setup for dynamic modulus of elasticity test.
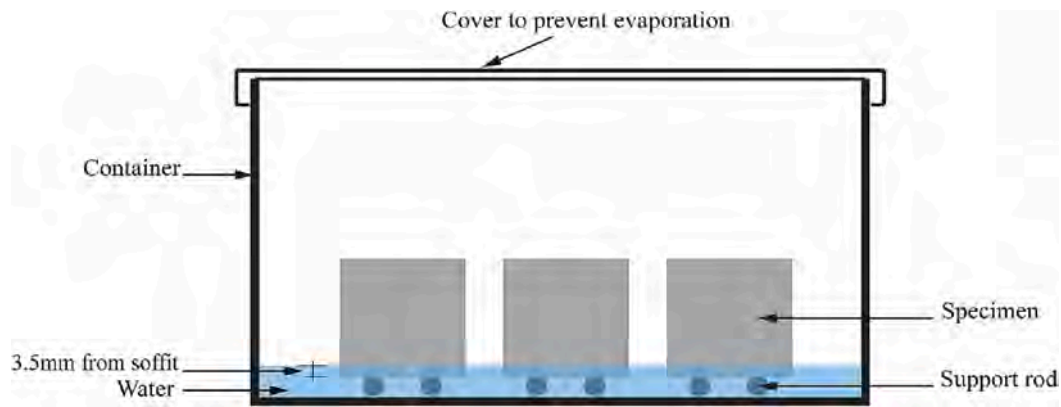
Fig. 7. Schematic diagram for water absorption test setup [32].

where n' = fundamental longitudinal frequency, Hz; M = mass of specimens, kg; and $D = 4 (L/bt)$, m^{-1} for a prism (L is the length, b, and t are dimensions of the cross-section).

2.7. Expansion test

As prescribed by ASTM C1260 [38], the study used the accelerated mortar bar test method to measure the linear expansion of $25 \times 25 \times 285$ mm^3 ($1 \times 1 \times 11.25$ in^3) mortar prisms under ASR conditions in a 1 N NaOH solution and stored in an oven at 80 °C (176 °F). The average length change of three mortar prisms was used as the representative value for each mixture composition. Daily measurement of the length change of each sample was performed for 14 days and left until the 28th day under the solution to record its length change. The length change of the samples (ΔL) was calculated as follows:

$$\Delta L = \frac{L_x - L_i}{G} \times 100\% \qquad (2)$$

where L_x = comparator reading of specimen at age x minus comparator reading of reference bar at age x, L_i = initial comparator reading of specimen minus comparator reading of reference bar at the given time, and G = nominal length of the mortar bar (G = 10 in. or 250 mm).

2.8. Water absorption test

The water absorption test was performed on the $50 \times 50 \times 50$ mm^3 mortar cube samples (28 days old) following the ASTM C1403 [39]. Before the test, the samples were dried in an oven at 80 ∘C for 24 h and then for 2 h until two successive weight measurements were not greater than 0.2% of the previous. Subsequently, the oven-dried samples were supported with rods in a sealed container with water, about 3.5 mm above the soffit of the samples. Fig. 7 shows a schematic diagram for the water absorption test. The weight of the samples was measured at intervals of 0.25, 1.00, 4.00, and 24.00 h after water exposure. The water absorption, A_T (g/100 cm^2), at each time interval was calculated using Eq. 3.

$$A_T = \frac{(W_T - W_O) \times 10000}{(L_1 \times L_2)} \qquad (3)$$

where W_T and W_0 are the samples' weights at time T and initial weight (measured in grams), respectively. Moreover, L_1 and L_2 are the average length and width of the samples (in mm).

2.9. Optical microscopy test

The microstructures of the mortar bars after 28 days under ASR-simulated conditions were observed and studied using optical microscopy (OM). In OM, thin slices with a cross-section of 25×25 mm^2 were cut from the mortar bars. First, a sodium cobaltinitrite-based ASR detection reagent was applied to the cross-section, waiting for 2 min. After that, the slice surface was washed with distilled water and dried for microscopic study. This reagent leaves a bright yellow precipitate if there is an initial stage of ASR degradation. In a second round, a rhodamine B detection reagent (for advanced ASR degradation) was also applied to the cross-sections and then washed and dried for OM observations.
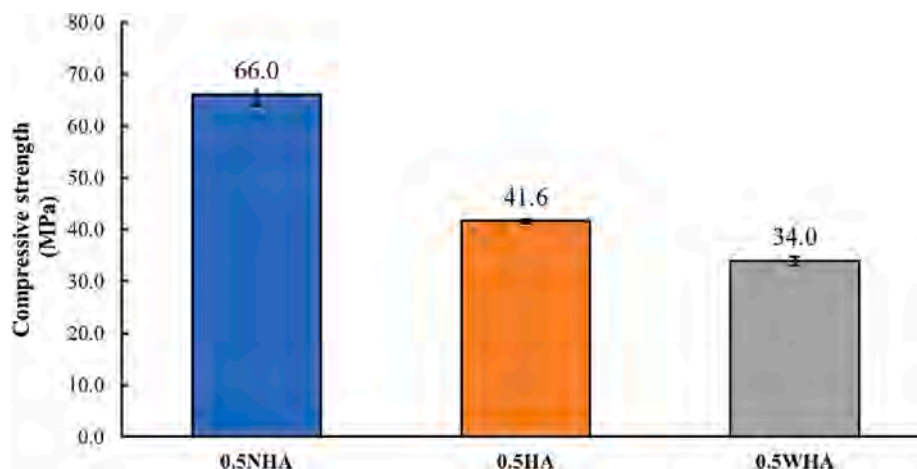
Fig. 8. 28-day compressive strength of samples.
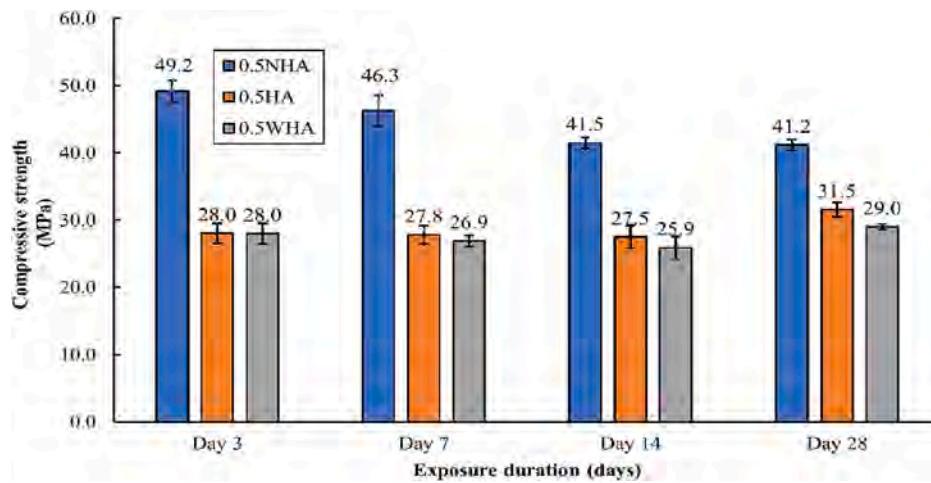
Fig. 9. Compressive strength of specimens exposed to ASR conditions.

2.10. Scanning electron microscopy test

The microstructures of the mortar bars after 28 days under ASR-simulated conditions were also observed and studied using scanning electron microscopy (SEM). In SEM, VEGA3 provided by TESCAN equipped with EDX was used. After being exposed to the ASR-simulated conditions for 28 days, mortar samples with sizes of approximately 5 mm × 5 mm × 3 mm were cut and submerged in the 2-Propanol solution for five days to stop hydration. These samples were then dried in an oven at 60° C for 24 h. Next, the samples were polished with p120, p240, p320, p600, and p1200 grits. Afterward, the polished specimens were washed using a sonicatic bath, and then dried. All specimens were sputter-coated with gold to suppress charging for better imaging quality. The secondary electron detector was selected during testing, with a voltage of 10 kV.

3. Results and discussion

3.1. Compressive strength

Fig. 8 presents the 28-day compressive strength of the mixture compositions exposed to 22 °C and 95% RH. The control samples registered the highest compressive strength (66.0 MPa), which was followed by 0.5HA (41.6 MPa) and 0.5WHA (34.0 MPa). This decline indicates that coating the aggregates reduces the compressive strength of the mortar, which can be due to inadequate bonding between the paste matrix and the coated aggregates and some negative impacts on cement hydration.

Fig. 9 shows the compressive strengths of samples under the ASR-simulated conditions for exposure days 3, 7, 14, and 28, respectively. Mortars with or without hydrophobic aggregates behaved differently with the continuous ASR deterioration. For instance, the compressive strength of 0.5NHA (control sample) decreased from 49.2 MPa on day 3 to 46.3 MPa on day 7 and 41.2 MPa on day 28, representing a 16.26% reduction. However, for both 0.5HA and 0.5WHA, the compressive strength stays roughly constant throughout the testing period and may
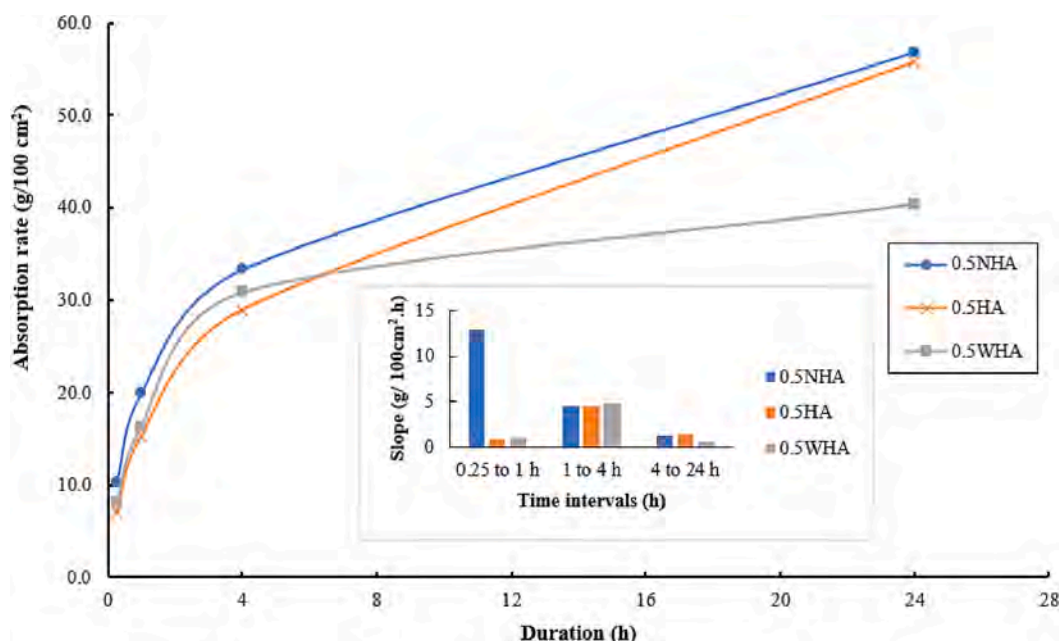
Fig. 10. Water absorption curves of the mortar samples.
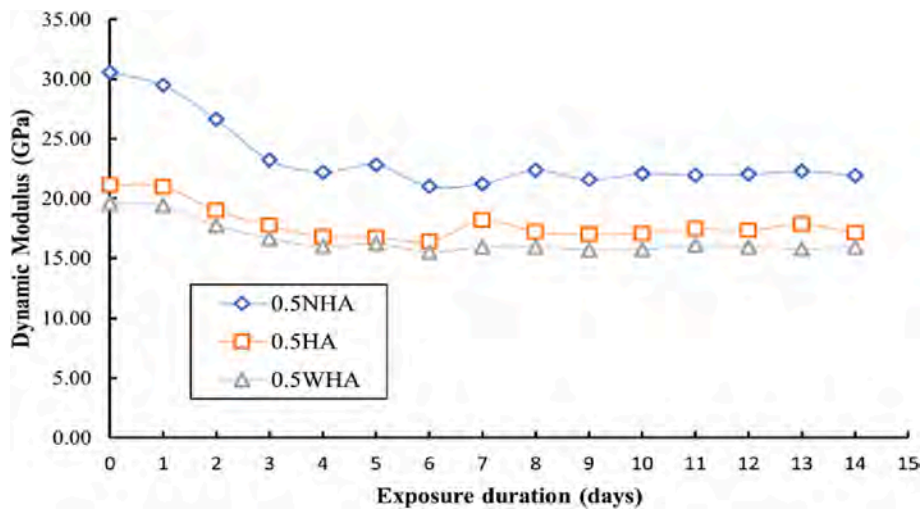
Fig. 11. Dynamic modulus of elasticity of specimens exposed to ASR conditions.

even slightly increase at 28 days. For example, strengths started from 28 MPa for 0.5HA and 0.5WHA at three days of ASR exposure and were maintained at this level for 14 days. Then, the strength slightly improved to 31.5 MPa for 0.5HA at 28 days (a 12.5% increase) and 29 MPa for 0.5WHA (3.5% increase compared to day 3). This occurrence can be a good indication of the prevention effect of hydrophobic sand on ASR deterioration. If the strengths of 28-day ASR exposure (in Fig. 9) are compared to the 28-day compressive strength under conventional curing conditions (in Fig. 8), one can see that the strengths have been retained at 62%, 76%, and 85%, respectively for 0.5NHA, 0.5HA, and 0.5WHA. The higher retaining rate indicates ASR prevention using hydrophobic aggregates and could be attributed to less expansion and internal cracking in the mortar.

3.2. Water absorption

Fig. 10 shows the curves for the water absorption rate of the mortar cubes, 0.5NHA, 0.5HA, and 0.5WHA, with each data point representing the average of three samples. The figure also shows the slope of the curves calculated at intervals of 0.25 to 1.0 h, 1.0 to 4.0 h, and 4.0 to 24.0 h. The capillary water absorption can indicate the effect of

hydrophobic aggregates on the moisture uptake of the mortar samples. Based on Fig. 10, the effect of incorporating hydrophobic aggregates in mortar may be explained in two ways. First, it can be observed that the samples with hydrophobic aggregates, both 0.5HA and 0.5WHA, had lower water absorption rates relative to the control (0.5NHA), especially for 0.5WHA, which has a much lower absorption rate at 24 h of water exposure. The lower water absorption rate can be attributed to the hydrophobic aggregates' capillary water-repelling ability in the mortar [26,32]. Also, incorporating hydrophobic aggregates in the mortar samples lengthened the moisture paths by increasing its tortuosity, reducing and slowing the moisture uptake. This assertion is evidenced by the rate of moisture ingress, indicated by the slope of the curves. At 0.25 to 1.0 h, the 0.5NHA absorbs moisture much quicker than 0.5HA and 0.5WHA. Although the absorption speed for all three mixtures stays on a similar level from 1.0 to 4.0 h, the 0.5WHA again shows the slowest water absorption compared to the other two from 4 to 24.0 h.

3.3. Dynamic modulus of elasticity

Fig. 11 shows the dynamic moduli of the various mortar prisms after their exposure to ASR conditions for 14 days, with each data point
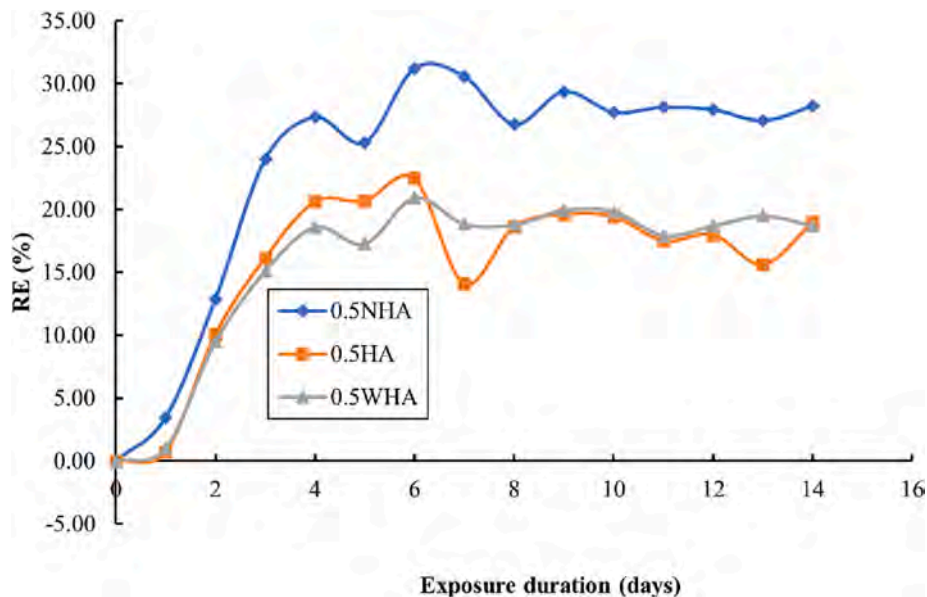
Fig. 12. Relative dynamic modulus of specimens as a function of exposure duration.
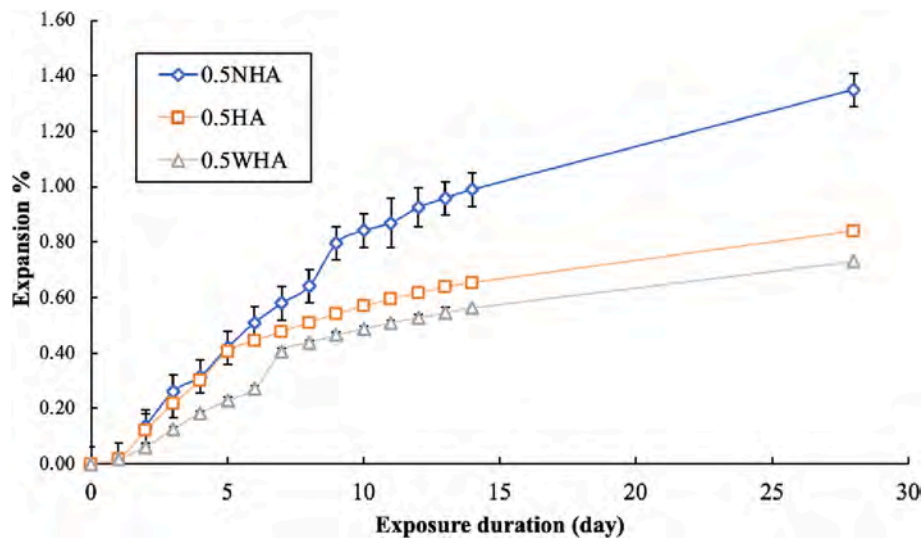
Fig. 13. Linear expansion curves of specimens under ASR conditions.

representing the average dynamic moduli of two prisms. From the curves, the dynamic moduli of all the mixture compositions decreased after day one exposure to the ASR conditions. The reduction in moduli is more noticeable for the first four to five days of subjection to ASR conditions, after which they remained relatively constant until the end of the testing period.

To further investigate the specimens' ASR deterioration, the dynamic modulus reduction is calculated using Eq. 4, where E_t represents dynamic modulus at the given age, and the E_o, corresponding dynamic modulus at zero reading of the given specimen (right before the exposure to ASR condition). The reduction in the dynamic elastic modulus indicates the extent of deterioration, such as microcracks and visible cracks in the mortar prisms [40].

$$RE = \left(1 - \frac{E_t}{E_o}\right) \times 100\% \tag{4}$$

Fig. 12 shows the reduction in dynamic moduli of the mix compositions under ASR conditions. Like the compressive strength, the control samples (0.5NHA) recorded the highest decline in the modulus compared to their hydrophobic counterparts (0.5HA and 0.5WHA). This reduction demonstrates that the control sample may have more severe cracks than the other two counterparts, as the dynamic modulus measurement is sensitive to crack initiation, propagation, and severity. The lower reduction rate of the 0.5HA and 0.5WHA can be attributed to reduced moisture uptake due to the hydrophobic layer on the aggregates, reducing the amount of ASR gel to cause deterioration [32]. Low moisture uptake into the ASR gel reduces swelling and subsequent crack formation in the microstructure of the specimens [18], thereby reducing the loss rate of the dynamic modulus of 0.5HA and 0.5WHA. This observation suggests that the hydrophobic aggregates effectively mitigate the effect of ASR on mortar.

3.4. ASR-induced expansion

Fig. 13 shows the expansion of the mortar prisms under the ASR conditions, with each data point representing the average linear expansion measurement of three prisms for each mixture composition. Generally, all the samples recorded expansion after their exposure, increasing as they continued to stay in the ASR-simulated condition. For example, after 14 days of exposure, 0.5NHA, 0.5HA, and 0.5WHA recorded expansions were 0.99, 0.65, and 0.56% for 0.5NHA, 0.5HA, and 0.5WHA, respectively. Furthermore, the 28th-day expansion values are 1.35, 0.84, and 0.73% for 0.5NHA, 0.5HA, and 0.5WHA. On both the

Fig. 14. Cracks developed on the surfaces of mortar bars under ASR conditions.

14th and 28th day, the expansion values of the control samples exceeded their hydrophobic counterparts, 0.5HA and 0.5WHA, confirming that using hydrophobic aggregates in mortar is beneficial for ASR prevention. The reduced expansion of 0.5HA and 0.5WHA can be ascribed to the hydrophobic layer on the surface of the aggregates, impeding moisture migration into ASR gel, formed on the face, or within aggregates to cause swelling. It is also noted that the expansion value at 14 days largely exceeds the reference value of the ASTM C1260 standard for potentially reactive aggregates (0.2%) [38], indicating that hydrophobic aggregates do not completely prevent the ASR expansion. This phenomenon can be attributed to the extremely high reactivity of aggregates used in this study. Notably, the 0.5WHA (approximately 14% lower) expanded at a lower rate than 0.5HA, indicating that washing the
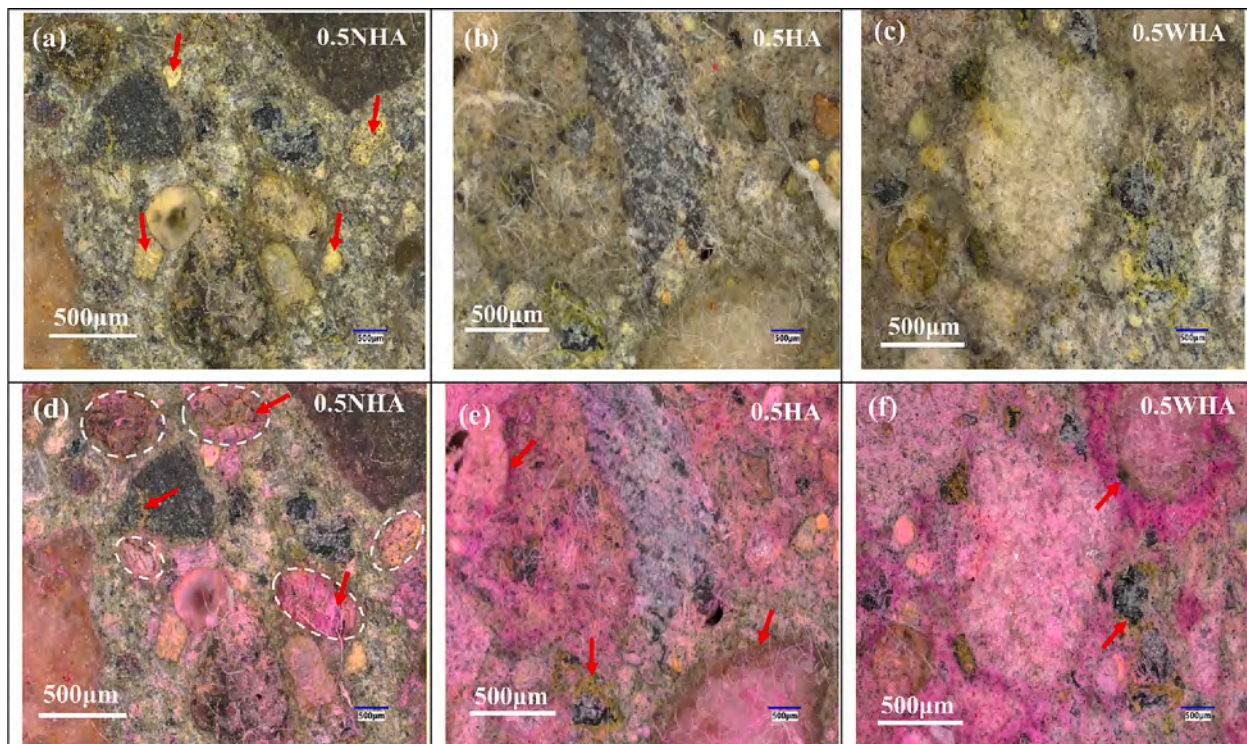
Fig. 15. Typical images of ASR-affected sample after 28 days of exposure.

surface of the aggregates before the hydrophobic coating is beneficial. Washed aggregates may possess a cleaner surface to receive the hydrophobic coating, thereby ensuring a better bonding of the hydrophobic silica with the aggregate surface. The improved bonding enhances the effectiveness of the hydrophobic aggregates to reduce moisture uptake, fostering a reduced expansion.

3.5. Cracking and deformation

During the ASR expansion tests, it was noticed that with the progress of ASR, cracks began to form, develop and be noticeable on the surfaces of the samples. For example, cracks began developing on the surfaces of 0.5NHA specimens after five days in the 1 N NaOH solution. In contrast, it took eight days before cracks appeared on the 0.5HA and 0.5WHA mortar bars. The delay in crack development on the samples with hydrophobic aggregates is another plausible example of the prevention of ASR deterioration with hydrophobic aggregates. This crack development delay is because the aggregates' hydrophobicity hinders the moisture migration into the ASR gel for swelling and subsequent cracking [3,24]. After 28 days of ASR-simulated exposure, more cracks were found on 0.5NHA than those on 0.5HA and 0.5WHA, evidenced in Fig. 14. During the expansion tests, it was also noticed that the control beam warped to some extent. The settlement of these expansive sands to the bottom of the beam may cause an uneven beam expansion across its depth. While warping has not been observed in those beams with treated sand.

3.6. Optical microscopic observation

Fig. 15 shows samples' OM images after exposure to ASR conditions for 28 days. The figure's first row captures the cross-section of the specimens after applying the sodium cobaltinitrite reagent. In Fig. 15(a), many bright yellowish stains can be observed on the surface of the cross-section, particularly at locations where the arrows point. These stains indicate the existence of gel containing potassium (K) ions [41]. Compared to Fig. 15(b) and Fig. 15(c), the yellowish stains are more

observable in the control specimens than in their hydrophobic counterparts (0.5HA and 0.5WHA), indicating the presence of more ASR gel to cause higher deleterious expansion. Among the three, 0.5WHA has the least yellow pigmentation, which qualitatively tells the least ASR deterioration of the specimen.

Fig. 15(d), 15(e), and 15(f) show the mortar surfaces after applying rhodamine B. Yellow and pink stains were observed not only at the boundaries but also through the aggregates of the control specimen, as shown in Fig. 15(d), with circles. However, the yellowish and pink stains were mainly observed at the peripheries of the hydrophobic aggregates, with arrows pointing at them in Fig. 15(e) and Fig. 15(f). In theory, these stains indicate the advancement of alkali-silica reactivity in the samples [41]. In Fig. 15(d), there are cracks in the aggregates (see red arrows), possibly resulting from ASR expansion. However, no apparent cracks are observed in the mortars with hydrophobic aggregates. These observations suggest that the control sample performed worse than its hydrophobic counterparts. Mainly observing ASR at the boundaries of the specimens with hydrophobic aggregates may be attributed to hindered moisture transport [32], which could carry alkalis to the aggregates' boundaries. It is important to note that these stains may not necessarily indicate the presence of harmful ASR gel, and further assessment methods should be used to characterize the gel [41]. Nonetheless, these findings further indicate the effectiveness of mitigating ASR in the mortar with hydrophobic aggregates.

3.7. SEM analysis

The SEM images of the samples after 28 days of exposure to ASR conditions are shown in Fig. 16. Generally, microcracks formed in all the specimens due to ASR gel expansion. However, the observation of the control (0.5NHA) mortars revealed a significant number and broader microcracks than those in the samples with hydrophobic aggregates. This can be seen by comparing Fig. 16(a), 16(c), and 16(e). These observations agree with the ASR-induced expansions discussed earlier, where the control samples attained much higher expansion than 0.5HA and 0.5WHA.
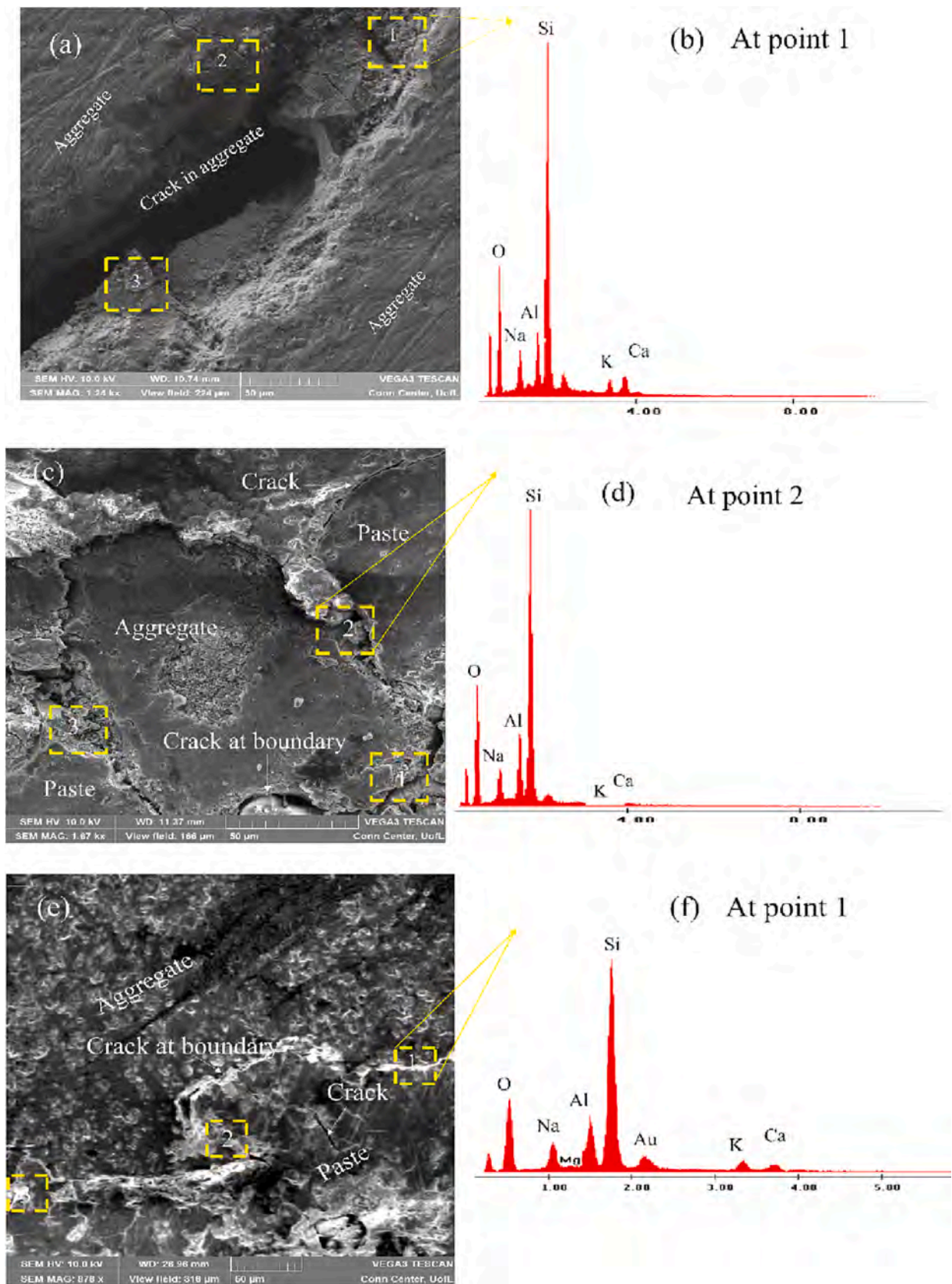
Fig. 16. SEM micrographs of (a) 0.5NHA, (c) 0.5HA, (e) 0.5WHA and corresponding EDX spectra (b) 0.5NHA, (d) 0.5HA, (f) 0.5WHA.

Table 3
Elemental composition of ASR-affected regions.

Mix ID	Composition (At %)					
	Si	Na	K	Ca	Ca/Si	(Na + K)/Si
0.5NHA	24.20 ± 2.58	13.3 ± 3.94	0.95 ± 0.18	1.88 ± 0.76	0.08 ± 0.03	0.59 ± 0.21
0.5HA	25.06 ± 0.92	9.62 ± 1.13	1.31 ± 0.20	0.89 ± 0.70	0.04 ± 0.03	0.44 ± 0.06
0.5WHA	25.31 ± 1.05	7.63 ± 1.09	1.02 ± 0.09	1.38 ± 1.34	0.06 ± 0.06	0.34 ± 0.04

For each sample, EDX spectra were taken at least three different locations. Sample EDX spectra for 0.5NHA, 0.5HA, and 0.5WHA are shown in Fig. 16(b), Fig. 16(d), and Fig. 16(f), respectively. All the spectra show that the most prevalent element is Si, with minor Na, K, Al, and Ca peaks. These observations correlate to ASR products in studies such as [42,43], primarily found at the boundaries of the aggregates. Table 3 captures the EDX elemental composition of ASR-affected regions of the various mixture compositions. Although similar chemical compositions were observed in the specimens, there were differences in the Ca/Si and (Na + K)/Si ratios from Table 3. Higher content of Ca^{2+} ions in the pore solution of the matrix contributes to the development of expansive ASR gel [4,43–45], suggesting that 0.5NHA had higher expansion than its hydrophobic counterparts.

Moreover, the (Na + K)/Si ratio of 0.5NHA is also higher than the samples with hydrophobic aggregates (0.5HA and 0.5WHA). An increase in (Na + K)/Si ratio in the ASR gels increases the free swelling of gels, and water uptake also increases, which may lead to higher ASR-induced expansion [4,43,46]. Indeed, the lower alkaline content at aggregate and crack surfaces in 0.5HA and 0.5WHA may be attributed to a disruption in their transport in the presence of the hydrophobic layer, limiting the extent of silica dissolution and ASR formation. These EDX results are other quantitative verification of the effectiveness of ASR prevention with hydrophobic aggregates.

4. Conclusions

This study explored the feasibility of mitigating the ASR deterioration in cement mortar using hydrophobic aggregates. The following conclusions have been made based on the findings of the study:

- Using hydrophobic aggregates might reduce the compressive strength of the mortar. However, the aggregate's hydrophobicity helps retain the relative strength (compared to the reference) when the material is subject to severe ASR conditions.
- Incorporating hydrophobic aggregates in the cement mortar improved the capillary water absorption properties of the mortar cubes compared to the control sample. In addition, the absorption rates were slower in the samples with hydrophobic aggregates, which can be attributed to the changes in the moisture paths within the system.
- Although the dynamic moduli of all mortar samples declined sharply after four days of exposure to ASR conditions, the decrement in the dynamic moduli of the samples produced with hydrophobic aggregates was moderate under ASR conditions, indicating good prevention of ASR-induced deteriorations.
- The mortar bar expansion test showed that hydrophobic aggregates could significantly reduce the expansion induced by ASR. It could also be concluded that using hydrophobic aggregates can delay crack initiation, reduce crack propagation, and reduce the warping/curling of the specimens.
- Both optical and scanning electron microscopy showed that hydrophobic aggregates could effectively reduce ASR deterioration. EDX results also show that changing aggregate surface hydrophobicity

alters the alkali pore solutions' transport, thus mitigating the expansion effectively.

Declaration of Competing Interest

The authors declare that they have no known competing financial interests or personal relationships that could have appeared to influence the work reported in this paper.

Data availability

Data will be made available on request.

References

[1] M. G. Alexander, "Developments in the Formulation and Reinforcement of Concrete," in *Woodhead Publishing Series in Civil and Structural Engineering*, S. Mindess Ed., Second Edition ed. United Kingdom: Woodhead Publishing, 2019, ch. 4, pp. 87-113.

[2] S.R. Paudel, M. Yang, Z. Gao, pH level of pore solution in alkali-activated fly-ash geopolymer concrete and its effect on ASR of aggregates with different silicate contents, J. Mater. Civ. Eng. 32 (9) (2020) 1–12, https://doi.org/10.1061/(ASCE) MT.1943-5533.0003344.

[3] R. Esposito, M.A.N. Hendriks, Literature review of modelling approaches for ASR in concrete: a new perspective, Eur. J. Environ. Civ. Eng. 23 (11) (2017) 1311–1331.

[4] R.B. Figueira, et al., Alkali-silica reaction in concrete: Mechanisms, mitigation and test methods, Constr. Build. Mater. 222 (2019) 903–931, https://doi.org/10.1016/ j.conbuildmat.2019.07.230.

[5] M. Zhang, W. Zhang, Y. Sun, Durability of concrete with nano-particles under combined action of carbonation and alkali silica reaction, J. Asian Architect. Build. Eng. 18 (5) (2019) 421–429, https://doi.org/10.1080/13467581.2019.1677470.

[6] D. Jóźwiak-Niedźwiedzka, A. Antolik, Assessment of highway pavement concrete suffering from alkali-silica reaction: case study, Mater. Constr. 72 (348) (2022) e299–e.

[7] M. Zeidan, A.M. Said, Effect of colloidal nano-silica on alkali–silica mitigation, J. Sustain. Cement-Based Mater. (2016) 1–13, https://doi.org/10.1080/ 21650373.2016.1191387.

[8] M. Zhang, W. Zhang, F. Xie, Experimental study on ASR performance of concrete with nano-particles, J. Asian Architect. Build. Eng. 18 (1) (2019) 3–9, https://doi. org/10.1080/13467581.2019.1582420.

[9] L. Kalina, V.B. Jr, L. Bradová, L. Topolář, Blastfurnace hybrid cement with waste water glass activator: alkali-silica reaction study, Materials 13 (3646) (2020) 1–9, https://doi.org/10.3390/ma13163646.

[10] F. Rajabipour, E. Giannini, C. Dunant, J.H. Ideker, M.D.A. Thomas, Alkali–silica reaction: Current understanding of the reaction mechanisms and the knowledge gaps, Cem. Concr. Res. 76 (2015) 130–146, https://doi.org/10.1016/j. cemconres.2015.05.024.

[11] D. Luo, A. Sinha, M. Adhikari, J. Wei, Mitigating alkali-silica reaction through metakaolin-based internal conditioning: New insights into property evolution and mitigation mechanism, Cem. Concr. Res. 159 (2022,), 106888, https://doi.org/ 10.1016/j.cemconres.2022.106888.

[12] K. Kobayashi, Y. Takagi, Penetration of Pressure-injected Lithium Nitrite in Concrete and ASR Mitigating Effect, Cem. Concr. Compos. (2020) 1–28, https:// doi.org/10.1016/j.cemconcomp.2020.103709.

[13] J.L. Lindgård, E.J. Sellevold, M.D.A. Thomas, P.B.H. Justnes, T.F. Rønning, Alkali–silica reaction (ASR)—performance testing: influence of specimen pre-treatment, exposure conditions and prism size on concrete porosity, moisture state and transport properties, Cement & Concr. Res. 53 (2013) 145–167, https://doi. org/10.1016/j.cemconres.2013.05.020.

[14] A. Leemann, Raman microscopy of alkali-silica reaction (ASR) products formed in concrete, Cem. Concr. Res. 102 (2017) 41–47.

[15] M. Shakooriooskooie, M. Griffa, A. Leemann, R. Zboray, P. Lura, Quantitative analysis of the evolution of ASR products and crack networks in the context of the concrete mesostructure, Cem. Concr. Res. 162 (2022), 106992, https://doi.org/ 10.1016/j.cemconres.2022.106992.

[16] M. D. Thomas, K. J. Folliard, B. Fournier, P. Rivard, T. Drimalas, and S. I. Garber, "Methods for Evaluating and Treating ASR-Affected Structures: Results of Field Application and Demonstration Projects: Volume II-Details of Field Applications and Analysis," United States. Federal Highway Administration, 2013.

[17] S. Multon, F. Toutlemonde, Effect of moisture conditions and transfers on alkali silica reaction damaged structures, Cem. Concr. Res. 40 (6) (2010) 924–934, https://doi.org/10.1016/j.cemconres.2010.01.011.

[18] M.-A. Bérubé, D. Chouinard, M. Pigeon, J. Frenette, L. Boisvert, M. Rivest, Effectiveness of sealers in counteracting alkali-silica reaction in plain and air-entrained laboratory concretes exposed to wetting and drying, freezing and thawing, and salt water, Can. J. Civ. Eng. 29 (2) (2002) 289–300.

[19] R. Al-Rashed, M. Al-Jabari, Concrete protection by combined hygroscopic and hydrophilic crystallization waterproofing applied to fresh concrete, Case Studies Constr. Mater. 15 (2021), https://doi.org/10.1016/j.cscm.2021.e00635 e00635.

[20] Z. Feng, F. Wang, T. Xie, J. Ou, M. Xue, W. Li, Integral hydrophobic concrete without using silane, Constr. Build. Mater. 227 (2019/12/10/ 2019,), 116678, https://doi.org/10.1016/j.conbuildmat.2019.116678.

[21] G. Blight, A study of four waterproofing systems for concrete, Mag. Concr. Res. 43 (156) (1991) 197–203.

[22] C. Zhang, S. Zhang, J. Yu, X. Kong, Water absorption behavior of hydrophobized concrete using silane emulsion as admixture, Cem. Concr. Res. 154 (2022), 106738.

[23] M.J. Al-Kheetan, M.M. Rahman, D.A. Chamberlain, Development of hydrophobic concrete by adding dual-crystalline admixture at mixing stage, Struct. Concr. 19 (5) (2018) 1504–1511.

[24] Z.Y. Qu, Q. Alam, F. Gauvin, T. Dezaire, H.J.H. Brouwers, F.Z. Wang, Development of water-resisting mortar by incorporation of functionalized waste incineration ashes, J. Clean. Prod. 249 (2020), 119341, https://doi.org/10.1016/j.jclepro.2019.119341.

[25] J. De Vries, R. Polder, Hydrophobic treatment of concrete, Constr. Build. Mater. 11 (4) (1997) 259–265.

[26] Z. Liu, W. Hansen, Effect of hydrophobic surface treatment on freeze-thaw durability of concrete, Cem. Concr. Compos. 69 (2016) 49–60, https://doi.org/10.1016/j.cemconcomp.2016.03.001.

[27] *Standard specification for Portland cement*, ASTM C150, West Conshohocken, PA, USA, 2009.

[28] *Standard test methods for chemical analysis of hydraulic cement*, ASTM C114, West Conshohocken, USA, 2015.

[29] H. Zhang, 4 - Cement, in: H. Zhang (Ed.), Building Materials in Civil Engineering, ch. 4, Woodhead Publishing, 2011, pp. 46–423.

[30] A. Rosli, A.L. Ahmad, S.C. Low, Enhancing membrane hydrophobicity using silica end-capped with organosilicon for CO2 absorption in membrane contactor, Sep. Purif. Technol. 251 (2020), 117429, https://doi.org/10.1016/j.seppur.2020.117429.

[31] K.-M. Li, J.-G. Jiang, S.-C. Tian, X.-J. Chen, F. Yan, Influence of silica types on synthesis and performance of amine–silica hybrid materials used for CO2 capture, J. Phys. Chem. C 118 (5) (2014) 2454–2462.

[32] K. Pasupathy, S. Ramakrishnan, J. Sanjayan, Effect of hydrophobic surface-modified fine aggregates on efflorescence control in geopolymer, Cem. Concr. Compos. 126 (2022), 104337.

[33] D. Lin-Vien, N.B. Colthup, W.G. Fateley, J.G. Grasselli, The handbook of Infrared and Raman Characteristic Frequencies Of Organic Molecules, Elsevier, 1991.

[34] T. Liu, H. Wei, A. Zhou, D. Zou, H. Jian, Multiscale investigation on tensile properties of ultra-high performance concrete with silane coupling agent modified steel fibers, Cem. Concr. Compos. 111 (2020), 103638.

[35] ASTM C305, "Standard practice for mechanical mixing of hydraulic cement pastes and mortars of plastic consistency ASTM C305-14," *ASTM Int. West Conshohocken PA,* 2014.

[36] ASTM C109, "ASTM C109-standard test method for compressive strength of hydraulic cement mortars," *ASTM International, West Conshohocken, PA,* 2008.

[37] ASTM C215, Standard test method for fundamental transverse, longitudinal, and torsional resonant frequencies of concrete specimens, Ann. Book ASTM Stand. (2019).

[38] ASTM C1260, ASTM C1260: Standard test method for potential alkali reactivity of aggregates (mortar–bar method), ASTM International, West Conshohocken, PA, USA, 2007.

[39] ASTM C 1403, *Standard Test Method for Rate of Water Absorption of Masonry Mortars1*. ASTM International, 2015.

[40] Z. Zhang, J. Olek, S. Diamond, Studies on delayed ettringite formation in early-age, heat-cured mortars: I. Expansion measurements, changes in dynamic modulus of elasticity, and weight gains, Cem. Concr. Res. 32 (11) (2002) 1729–1736.

[41] J.A. Farny, S.H. Kosmatka, Diagnosis and control of alkali-aggregate reactions in concrete, Portland Cement Association Skokie, IL, 1997.

[42] Z. Shi, C. Shi, R. Zhao, S. Wan, Comparison of alkali–silica reactions in alkali-activated slag and Portland cement mortars, Mater. Struct. 48 (3) (2015) 743–751.

[43] A. Leemann, G. Le Saout, F. Winnefeld, D. Rentsch, B. Lothenbach, Alkali–silica reaction: the influence of calcium on silica dissolution and the formation of reaction products, J. Am. Ceram. Soc. 94 (4) (2011) 1243–1249.

[44] T. Yang, Z. Zhang, Q. Wang, Q. Wu, ASR potential of nickel slag fine aggregate in blast furnace slag-fly ash geopolymer and Portland cement mortars, Constr. Build. Mater. 262 (119990) (2020) 1–9, https://doi.org/10.1016/j.conbuildmat.2020.119990.

[45] L. Kalina, V. Bílek Jr, L. Bradová, L. Topolář, Blastfurnace hybrid cement with waste water glass activator: alkali-silica reaction study, Materials 13 (16) (2020) 3646.

[46] A.K. Saha, M.N.N. Khan, P.K. Sarker, F.A. Shaikh, A. Pramanik, The ASR mechanism of reactive aggregates in concrete and its mitigation by fly ash: A critical review, Constr. Build. Mater. 171 (2018) 743–758, https://doi.org/10.1016/j.conbuildmat.2018.03.183.